

A hybrid approach for simulating fluid loading effects on structures using experimental modal analysis and the boundary element method

Micah R. Shepherd, John B. Fahnlne, Tyler P. Dare, et al.

Citation: *The Journal of the Acoustical Society of America* **138**, 3073 (2015); doi: 10.1121/1.4934959

View online: <https://doi.org/10.1121/1.4934959>

View Table of Contents: <https://asa.scitation.org/toc/jas/138/5>

Published by the [Acoustical Society of America](#)

ARTICLES YOU MAY BE INTERESTED IN

[Modal decomposition of exterior acoustic-structure interaction](#)

The Journal of the Acoustical Society of America **133**, 2668 (2013); <https://doi.org/10.1121/1.4796114>

[Analytical approximations for the modal acoustic impedances of simply supported, rectangular plates](#)

The Journal of the Acoustical Society of America **122**, 719 (2007); <https://doi.org/10.1121/1.2747094>

[Radiation Resistance of a Rectangular Panel](#)

The Journal of the Acoustical Society of America **51**, 946 (1972); <https://doi.org/10.1121/1.1912943>

[A lumped parameter model for the acoustic power output from a vibrating structure](#)

The Journal of the Acoustical Society of America **100**, 3539 (1996); <https://doi.org/10.1121/1.417330>

[Minimizing the acoustic power radiated by a fluid-loaded curved panel excited by turbulent boundary layer flow](#)

The Journal of the Acoustical Society of America **136**, 2575 (2014); <https://doi.org/10.1121/1.4896823>

[Sound radiation by a simply supported unbaffled plate](#)

The Journal of the Acoustical Society of America **103**, 2451 (1998); <https://doi.org/10.1121/1.422765>

JASA
THE JOURNAL OF THE
ACOUSTICAL SOCIETY OF AMERICA

Special Issue:
Additive Manufacturing and Acoustics

Read Now!

A hybrid approach for simulating fluid loading effects on structures using experimental modal analysis and the boundary element method

Micah R. Shepherd,^{a)} John B. Fahline, Tyler P. Dare, Stephen A. Hambric, and Robert L. Campbell

Applied Research Laboratory, The Pennsylvania State University, P.O. Box 30, State College, Pennsylvania 16804, USA

(Received 3 June 2015; revised 30 September 2015; accepted 19 October 2015; published online 17 November 2015)

Many structural acoustics problems involve a vibrating structure in a heavy fluid. However, obtaining fluid-loaded natural frequencies and damping experimentally can be difficult and expensive. This paper presents a hybrid experimental-numerical approach to determine the heavy-fluid-loaded resonance frequencies and damping of a structure from in-air measurements. The approach combines in-air experimentally obtained mode shapes with simulated in-water acoustic resistance and reactance matrices computed using boundary element (BE) analysis. The procedure relies on accurate estimates of the mass-normalized, *in vacuo* mode shapes using singular value decomposition and rational fraction polynomial fitting, which are then used as basis modes for the in-water BE analysis. The method is validated on a 4.445 cm (1.75 in.) thick nickel-aluminum-bronze rectangular plate by comparing natural frequencies and damping obtained using the hybrid approach to equivalent data obtained from actual in-water measurements. Good agreement is shown for the fluid-loaded natural frequencies and one-third octave loss factors. Finally, the limitations of the hybrid approach are examined. © 2015 Acoustical Society of America.
[<http://dx.doi.org/10.1121/1.4934959>]

[KML]

Pages: 3073–3080

I. INTRODUCTION

A fluid in contact with a structure will impart a complex impedance loading on that structure. The resistance will create additional damping from the acoustic radiation, while the reactance will generally cause mass-loading. Several examples where fluid loading is important include ship hulls, sonar transducers, liquid-filled pipes, liquid-cooled nuclear reactor internals, and sandwich honeycomb panels. Unbounded fluids act mostly as inertial loading, while enclosed fluids may exhibit inertial or elastic loading.

Heavy external fluids such as water and oil will decrease natural frequencies of a vibrating structure due to the extra force required to accelerate the fluid's inertia. By estimating the mass loading of the fluid surrounding the structure and knowing the unloaded natural frequencies, estimates for the fluid-loaded resonance frequencies can be obtained. Approximate equations for the shift in resonance frequency can be found for example in Leissa¹ or Blevins.² In addition to the shift in natural frequency, heavy fluid loading can lead to a change in the radiation pattern for a point-driven plate, causing the radiation to become more “dipole-like.”³ Radiation damping can also be significant for thick, lightly damped structures, particularly near the coincidence frequency of flexural and acoustic waves. Thus, knowing the effects of heavy fluid loading on vibro-acoustic behavior of a structure is critical.

Separating structural damping from acoustic damping is also critical for modeling purposes, which often rely on measurements for correct damping values. The damping obtained from a measurement will include the combined effects of both structural and acoustic radiation damping. If the acoustic radiation damping is not removed, a vibration model using uncorrected damping may be over-damped and predict incorrect vibration levels.

Measurements on fully submerged structures are much more difficult and time consuming than the in-air equivalent. Installation and general use of transducers can be more tedious, and structures are typically more difficult to excite, particularly when using a force hammer. Also, many underwater measurements require large bodies of water, typically a water tank or lake, and certified divers, which can be a large liability and expense. Additionally, the existence of reflections from the water-air surface or tank boundaries could create error under some circumstances. These difficulties limit the amount of design testing and model validation that can be performed.

This paper will discuss a hybrid experimental-numerical approach for computing the heavy-fluid-loading effects on a structure using in-air measurements and acoustic boundary element (BE) analysis. Experimental modal analysis (EMA) is used to assess the modal parameters of the structures and a lumped parameter BE technique is used to compute the fluid loading. The procedure relies on accurate estimates of the mass-normalized mode shapes from experimental modal analysis in air, which are then used as basis modes for the BE analysis. The hybrid approach is demonstrated on a

^{a)}Electronic mail: mrs30@psu.edu

4.445 cm (1.75 in.) thick nickel-aluminum-bronze (NAB) panel by comparing simulated natural frequencies and damping to equivalent data obtained from actual in-water measurements. The results compare well, validating the hybrid approach.

II. TEST STRUCTURE

A thick NAB plate of dimensions 762 mm × 305 mm × 44.4 mm (30 in. × 12 in. × 1.75 in.) was used to validate the hybrid approach. The density of the plate is approximately 7468 kg/m³. To simulate free boundary conditions, the plate was suspended vertically using 100-lb test fishing line threaded through 4 small holes at each corner. The holes were drilled through the thickness of the plate, approximately 1.8 cm in from each corner. Modal analysis was performed on the panel in air and then repeated in water.

Four small accelerometers (PCB Piezotronics, Inc. Depew, NY, W352-C67) were attached to the surface of the plate using cyanoacrylate adhesive at locations shown in Fig. 1. Using the roving hammer approach, the panel was excited with impulses at 0.0254 m (1 in.) intervals along the length and width of the panel for a total of 403 points (31 × 13). Acceleration to force frequency response functions (FRFs) were recorded at a sampling frequency of 12 800 Hz with three root-mean-square averages per hit location. The record time was varied to ensure that a sufficiently long time sample was recorded to capture the full decay of the structure, which sometimes reached 20 s due to the low material damping. The FRFs were collected with a 5% pre-trigger and carefully monitored to ensure high coherence existed at each measurement point.

The modal test was then repeated with the plate submerged in a reverberant water tank (8.7 m × 6.9 m × 5.5 m). A 0.0508 m (2 in.) spacing was used for a total of 112 hit points. Fewer points were used than in air due to the higher difficulty of obtaining data underwater. Water-resistant accelerometers and force hammer were used. The acquired data were processed to extract the modal parameters using the procedure outlined in Sec. III.

III. EXTRACTING MODAL PARAMETERS

The matrix of acceleration to force transfer functions was processed using the singular value decomposition, one frequency at a time. The data were arranged in matrix form with each column representing the response to a different

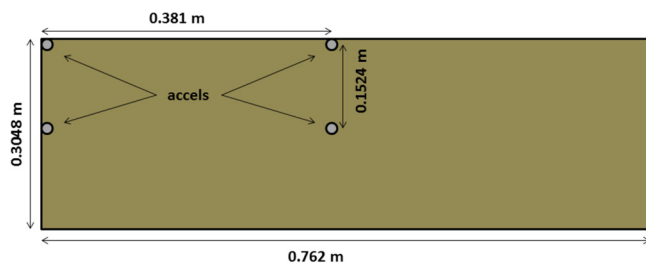


FIG. 1. (Color online) Schematic of the NAB plate used to validate the hybrid fluid loading approach. The plate was suspended to replicate free-free boundary conditions. Four accelerometers were placed on the structure for the measurements.

drive point and each row representing a different response point. The resulting matrix was input to the singular value decomposition algorithm, and left- and right-singular vectors and a diagonal singular value matrix were computed.⁴ Because they were computed and output in order of descending magnitude, one singular value curve does not track a single mode. It is possible to force the singular values to track only a single mode by using the singular value decomposition (SVD) at one frequency to decompose the coefficient matrix at nearby frequencies. The resulting functions were originally called “enhanced FRFs,”⁵ although the more descriptive name “modal transfer functions” is used here instead. To reduce computation times, the modal transfer functions were only calculated over a limited frequency range near the resonance peaks. The modal transfer functions separate the data well for the individual modes (see Fig. 2) even when the resonance frequencies are in close proximity.

The output from the singular value decomposition consists of three matrices, \mathbf{U} , \mathbf{V} , and \mathbf{S} . The \mathbf{U} and \mathbf{V} matrices are unitary (e.g., $\mathbf{U}\mathbf{U}^H = \mathbf{1}$, where the superscript H indicates a Hermitian transpose), and the \mathbf{S} matrix contains the singular values on its diagonal and is real-valued. The three matrices form a decomposition of the original matrix as

$$\mathbf{H}(\omega_0) = \mathbf{U}(\omega_0)\mathbf{S}(\omega_0)\mathbf{V}^H(\omega_0), \quad (1)$$

where ω_0 is the analysis frequency. Simple physical interpretations can be given to the \mathbf{U} and \mathbf{V} matrices. The matrix \mathbf{U} is of size (# response points) by (# drive points), and its columns (termed left-singular vectors) represent the vibration patterns associated with each of the singular values, and thus are interpreted as “unscaled mode shapes.” When we refer subsequently to “SVD mode shapes,” we really are referring to the left-singular vector associated with the singular value under consideration. The matrix \mathbf{V} is of size (# drive points) by (# drive points), and its columns (termed right singular vectors) represent the required input forces at the drive points to excite the left-singular vectors and is therefore discarded. In general, the \mathbf{U} and \mathbf{V} matrices do not change significantly from one frequency to the next, and thus most of

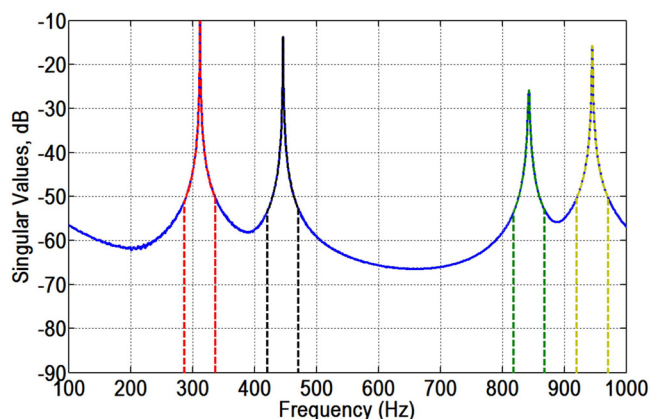


FIG. 2. (Color online) The modal parameters are estimated using modal transfer functions calculated at a limited number of frequencies surrounding the peak of interest. The first set of singular values is shown as a solid line while the individual modal transfer functions are shown as dashed curves. Away from the peaks, the singular values take on the value of zero.

the frequency dependence in the transfer function data are contained in the singular values. In this implementation, 128 frequency bins were used for each modal transfer function.

The SVD algorithm relegates noise to the lowest singular values, thus reducing the noise levels in the top few curves that typically contain most of the modal information. Unfortunately, the singular values are output from the decomposition in order of magnitude, so that they switch the modes they are tracking whenever two singular values cross. This problem is avoided by computing modal transfer functions, which force the singular values to track a single mode. These functions are computed by using the singular value decomposition at an initial frequency to decompose the transfer function matrix at nearby frequencies as

$$\bar{\mathbf{S}}(\omega) = \mathbf{U}^{\mathbf{H}}(\omega)\mathbf{H}(\omega)\mathbf{V}(\omega_0). \quad (2)$$

The overbar on the matrix \mathbf{S} indicates that it is no longer real-valued or diagonal. Savitz-Golay filters are applied to the data to reduce noise⁶ and the modal assurance criteria are used to detect duplicate modes. Once a peak is found, the modal parameters are then estimated using a linear least squares circle fit of the modal transfer function equation for a single mode.¹

While the scaling of the identified mode shapes is arbitrary, using mass-normalized mode shapes enables the measured data to be synthesized without knowledge of the system mass or stiffness characteristics. The transfer function between the displacement at node α due to an input force at node β (i.e., d_α/f_β) can be written in the form⁷

$$\begin{aligned} \frac{d_\alpha}{f_\beta} &= \sum_{\mu=1}^N \frac{\Phi_{\alpha\mu}\Phi_{\beta\mu}}{(k_\mu - \omega^2 M_\mu) + i \eta_\mu k_\mu} \\ &= \sum_{\mu=1}^N \frac{1}{M_\mu} \frac{\Phi_{\alpha\mu}\Phi_{\beta\mu}}{\omega_\mu^2 - \omega^2 + i \eta_\mu \omega_\mu^2}, \end{aligned} \quad (3)$$

where k_μ , M_μ , and η_μ are the stiffness, mass, and loss factor at mode μ and N is the number of modes. In Eq. (3), $\Phi_{\alpha,\mu}$ represents unscaled mode shapes, which are extracted from the SVD analysis as the left-singular vectors accompanying peaks in the singular values. When the drive and response point are the same, this reduces to

$$\frac{d_\alpha}{f_\alpha} = \sum_{\mu=1}^N \frac{1}{M_\mu} \frac{|\Phi_{\alpha\mu}|^2}{\omega_\mu^2 - \omega^2 + i \eta_\mu \omega_\mu^2}. \quad (4)$$

To derive the modal transfer functions, the transfer function matrix is multiplied by the corresponding left- and right-singular vectors at the peak, as in Eq. (2). In a similar fashion, it is possible to set all but one of the singular values to zero, and then calculate a “filtered” transfer function matrix at ω_0 containing the contribution from only singular value μ as

$$\mathbf{H}_\mu(\omega_0) = \sigma_\mu(\omega_0)\mathbf{u}_\mu(\omega_0)\mathbf{v}_\mu(\omega_0), \quad (5)$$

where \mathbf{u}_μ is of size (# Response Points \times 1) and \mathbf{v}_μ is of size (1 \times # Drive Points). The filtered transfer function data are

then consistent with the left-singular vectors, and the drive point transfer functions can be extracted from the matrix.

As long as the singular value decomposition is successful at separating the various modes from each other and accurate damping loss factors η_μ are extracted, the transfer function for a single mode can be approximated by a single term of the summation as

$$\frac{d_\alpha}{f_\alpha} = \frac{1}{M_\mu} \frac{|\Phi_{\alpha\mu}|^2}{\omega_\mu^2 - \omega^2 + i \eta_\mu \omega_\mu^2}, \quad (6)$$

and modal mass can now be computed. The mode shapes can be mass-normalized by dividing by the modal mass scale factor $T_\mu = 1/\sqrt{M_\mu}$. In theory, the calculation can be performed using any location where drive point transfer function data are available. However, the computations become inaccurate and unstable when the drive point location is near a nodal line. Thus, the modal mass is computed using the drive point with the largest response amplitude.

To refine the SVD estimates for the resonance frequencies and loss factors, the modal parameters are then updated using rational fraction polynomial (RFP) curve-fitting. The RFP algorithm is adapted from that given in Ref. 8. Residual contributions of nearby modes are accounted for using higher-order polynomial fits. The displacement data can then be synthesized once the resonance frequencies, loss factors, and mass normalized mode shapes have been determined.

The measurements required for experimental modal analysis also can be used to derive other useful information. One third octave loss factors based on the power injection method can be computed as $\eta_{\text{Pin}} = \text{Conductance}/(\omega \text{ Energy})$, where the conductance for a particular drive point location μ is simply the real component of the velocity divided by the input force, $\text{Re}\{v_\mu/F_\mu\}$.

The power injection and radiation loss factors require vibrational energy to be computed as a function of frequency. The energy can be computed directly given the incremental structural masses at each of the nodal locations as

$$E = \mathbf{v}^{\mathbf{H}}\mathbf{M}\mathbf{v} = \omega^2 \mathbf{d}^{\mathbf{H}}\mathbf{M}\mathbf{d}. \quad (7)$$

For this calculation to be performed, a mesh is created using the hit points from the modal analysis. Densities and thicknesses are defined for the mesh elements, thus assuming that a plate representation is appropriate. The energy is computed by assigning an incremental mass to each node, assuming the matrix M is diagonal, and then performing the calculation in Eq. (7). The overall mass at each node is computed by first calculating the element masses, and then assigning each connected node an equal portion of the mass and summing. This method can be difficult for inhomogeneous complex structures.

A second method for computing energy that does not require input for the element densities can also be used. The method assumes that the displacements can be represented in terms of a modal summation as

$$\mathbf{d} = \Phi \xi(\omega), \quad (8)$$

where the mode shapes are the columns of Φ and the vector ξ is made up of the modal participation factors. Assuming

the modes are orthogonal and mass normalized, the modal participation factors are given as

$$\xi_{\mu}(\omega) = \frac{1}{\omega_{\mu}^2 - \omega^2 + i \eta_{\mu} \omega_{\mu}^2} \Phi_{\mu}^T \mathbf{f}. \quad (9)$$

The energy can then be written as

$$\begin{aligned} E &= \mathbf{v}^H \mathbf{M} \mathbf{v} = \omega^2 \mathbf{d}^H \mathbf{M} \mathbf{d} \\ &= \omega^2 \xi^H(\omega) \Phi^H \mathbf{M} \Phi \xi(\omega) = \omega^2 \xi^H(\omega) \xi(\omega). \end{aligned} \quad (10)$$

It is desirable to use this method to compute energy not only because it does not require input for the elemental densities, but also because it can be generalized to structures that are not “plate-like.” Since the modal participation factors only depend on the mode shape amplitudes at the locations where forces are input to the system [due to the $\Phi_{\mu}^T \mathbf{f}$ term in Eq. (9)], the energy will be correct as long as they are normalized correctly. In general, if the surface displacements can be accurately synthesized using Eq. (8), then the energies will be computed accurately.

IV. COMPUTATION OF FLUID LOADING

Once the mass-normalized mode shapes are estimated, the fluid loading matrices can be determined. When fluid loading is added to a structural vibration model, the displacements \mathbf{d} satisfy

$$[\mathbf{K} - \omega^2 \mathbf{M} + \mathbf{A}(\omega)] \mathbf{d} = \mathbf{f}, \quad (11)$$

where \mathbf{K} and \mathbf{M} are the stiffness and mass matrices, respectively, \mathbf{A} is the acoustic coupling matrix, and \mathbf{f} is the input force.^{9,10} The matrix \mathbf{A} relates the generalized forces due to the acoustic pressure field to the nodal displacements and contains both resistive and reactive components. It can be generated using BE or finite element analysis or analytically for simple shapes. Using the principal of modal summation leads to a reduction in matrix size and requires an estimate of the modal acoustic coupling matrix $\Phi^T \mathbf{A} \Phi$. In this paper, the modal acoustic coupling matrix was computed using the lumped parameter method by Fahline and Koopman.^{11,12} The lumped parameter method has been recently used for optimization of a fluid-loaded panel.¹³

To accommodate these computations, the discrete hit points used in experimental modal analysis are used as grids which are connected to form elements and create a wetted surface mesh for numerical analysis. The modal coupling matrix is then determined using equivalent source amplitudes from each element (i.e., the lumped parameters method) and the experimentally-obtained mode shapes. In this application, the elements were treated as dipole sources since there is contact with the fluid on both sides of the plate.

The dipole sources were aligned in the normal direction of the plate in order to represent the pressure difference on the two sides and the dipole source amplitudes were determined by enforcing the boundary condition for the normal surface velocity. Since the plate is thin (i.e., small with respect to wavelength), the velocity at any particular point is exactly the opposite from the corresponding point on the back side. Consequently, only the top velocity boundary condition must be matched. A related discussion is found in Terai¹⁴ and Martinez.¹⁵

To ensure convergence of the numerical solutions, the mesh must be refined enough to resolve the acoustic waves. The typical rule of thumb for BE methods is to use six elements per wavelength for linear basis functions. Since the hit points were spaced at 0.0254 m (1 in.) apart in the modal analysis, the acoustic element length is also at 0.0254 m.

The BE model should then resolve acoustic waves up to 9.8 kHz. The characteristic impedance of water [1.5×10^{-6} kg/(s m²)] was used for the surrounding fluid. It should also be noted that the lumped parameter BE formulation has been shown to converge as a function of acoustic element mesh density.¹¹ The BE mesh is shown in Fig. 3.

V. HYBRID EXPERIMENTAL/NUMERICAL APPROACH

To compute the simulated in-water modal participation factors and resulting surface vibration, the numerical modal acoustic coupling matrix is included directly into the matrix form of Eq. (9),

$$[\xi] = [\omega_{\mu}^2 - \omega^2 + i \eta_{\mu} \omega_{\mu}^2 + \Phi^T \mathbf{A} \Phi]^{-1} \Phi_{\mu}^T \mathbf{f}. \quad (12)$$

The modal participation matrix is now fully populated due to the acoustic coupling matrix. The fluid-loaded power transfer function is then computed directly (without requiring surface vibrations) using

$$\Pi = \xi \mathbf{Re}\{\Phi^T \mathbf{A} \Phi\} \xi^T. \quad (13)$$



FIG. 3. (Color online) The BE mesh is created by connecting excitation points together into elements. Each element shade represents a separate dipole source whose amplitude is determined by matching the surface velocity boundary condition.

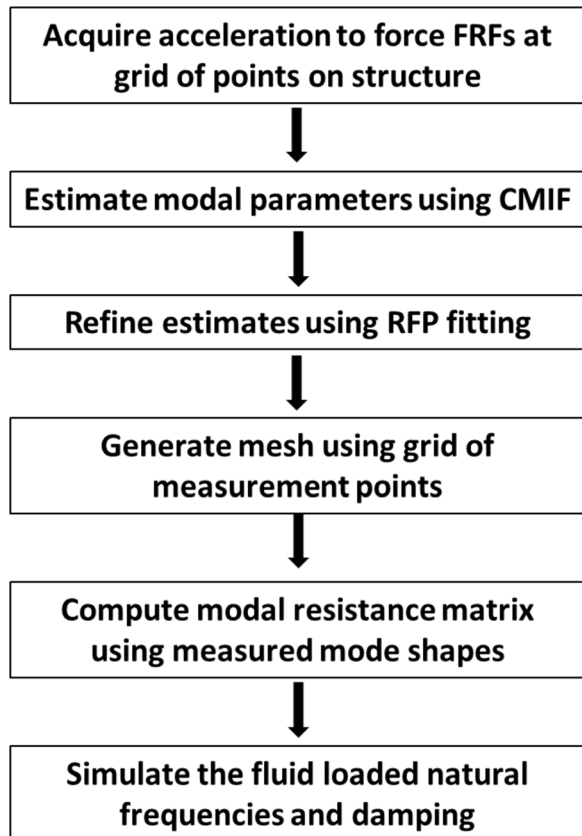


FIG. 4. A flow chart of the hybrid EMA/BE methodology.

This simulates the radiated sound power in the heavy fluid given a unit point drive at the accelerometer response points. According to reciprocity, the reference and response points can be exchanged to produce the same results. Additionally, acoustic radiation loss factors can be computed as $\eta_{\text{Pin}} = \text{Radiated Power}/(\omega \text{ Energy})$.

The fluid-loaded mode shapes could also be computed using a similar singular value decomposition approach described by Fahline¹⁶ or with other approaches such as the modal decomposition approach using polynomial approximations and eigenvalue linearization by Peters *et al.*^{17,18} These approaches follow the state space formulation originally posed by Giordano and Koopman.¹⁹ A flow chart describing the general approach is shown in Fig. 4.

VI. RESULTS

The modal parameters were determined for the NAB plate data measured in air using the procedure described in Sec. III. The natural frequencies and mode orders are listed in Table I. The theoretical dimensionless wavenumbers (kL) are also listed for free-free plates. Since the synthesis procedure relies on an accurate estimate of the mass-normalized mode shapes, the mass normalizations are also compared to those determined with a finite element model. The modal mass scale factor (fraction of plate static mass) is shown for the first eight modes in Table I with the associated percent difference. The percent error is highest for the lowest order mode but quickly becomes small for higher-order modes. The higher error in the first natural frequency may be an artifact of hanging the panel from fishing line instead of having a truly free boundary condition. The average modal mass scale factor is approximately 0.315 which is comparable to, but slightly higher than, the value of 0.25 for plates with simply-supported boundary conditions.²⁰

The first 17 natural frequencies obtained from in-air modal analysis are compared to those with simulated water loading and those obtained from the in-water modal analysis in Table II. Fluid loading causes a downward shift in resonance frequency of about 10%. The percent difference between the measured and simulated water loaded frequencies is also shown in Table II revealing good accuracy of the virtual fluid loading procedure. The largest difference is seen for the 1st mode and the 17th mode, which is less than 5%. Five measured mode shapes in air and in water are shown in Fig. 5.

Since the natural frequency of an elastic structure is inversely proportional to the square root of its mass, the effects of the fluid mass can be expressed approximately as

$$\frac{\omega_L}{\omega_v} = \frac{1}{\sqrt{1 + m_f/m_s}}, \quad (14)$$

where ω_L is the natural frequency of the fluid-loaded structure, m_f is the mass loading of the fluid, and m_s is the mass of the structure.² It should be noted that if the fluid mass changes the structural mode shape, this approximate form would not hold.

The modal damping of the plate in air is shown in Fig. 6. The damping levels are very small, between 6.0×10^{-5} and

TABLE I. Modal frequencies, wavenumbers, and experimentally-obtained estimates of the modal mass scale factors for the NAB plate in air.

Mode #	Exp. Freq. (Hz)	(m,n)	$k_x L_x$	$k_y L_y$	Exp. M_μ/M_{static}	FE estimated M_μ/M_{static}	% M_μ/M_{static} Difference
1	312	(2,0)	4.712	0.0	0.230	0.294	-27.8
2	446	(1,1)	1.571	1.571	0.295	0.330	-12.0
3	843	(3,0)	7.854	0.0	0.238	0.257	-8.1
4	945	(2,1)	4.712	1.571	0.326	0.329	-0.9
5	1552	(3,1)	7.854	1.571	0.346	0.352	-1.9
6	1601	(4,0)	10.99	0.0	0.269	0.273	-1.3
7	1880	(0,2)	0.0	4.712	0.285	0.274	6.8
8	2023	(1,2)	1.571	4.712	0.329	0.326	0.9
9	2308	(4,1)	10.99	1.571	0.345	0.335	2.9
10	2493	(2,2)	4.712	4.712	0.346	0.357	-3.0

TABLE II. Natural frequencies of the NAB plate measured in air, predicted with hybrid approach and measured in water.

In-air (Hz)	Water simulated (Hz)	% frequency shift	Water measured (Hz)	% difference
312	255	-18.27	268	4.85
446	396	-11.21	400	1.00
843	732	-13.17	741	1.22
945	848	-10.27	855	0.82
1552	1409	-9.21	1416	0.49
1601	1413	-11.74	1431	1.26
1880	1689	-10.16	1716	1.57
2023	1832	-9.44	1863	1.66
2308	2121	-8.10	2121	0.00
2493	2266	-9.11	2298	1.39
2592	2344	-9.57	2342	-0.09
3155	2875	-8.88	2914	1.34
3223	2978	-7.60	2979	0.03
3707	3389	-8.58	3378	-0.33
3958	3645	-7.91	3665	0.55
4276	3970	-7.16	3971	0.03
4650	4206	-9.55	4413	4.69

8.0×10^{-4} with a peak near 1 kHz. The peak damping is a result of in-air radiation damping at coincidence. The in-air coincidence frequency based on thick plate theory is 360 Hz. Due to the low modal overlap near coincidence, the radiation

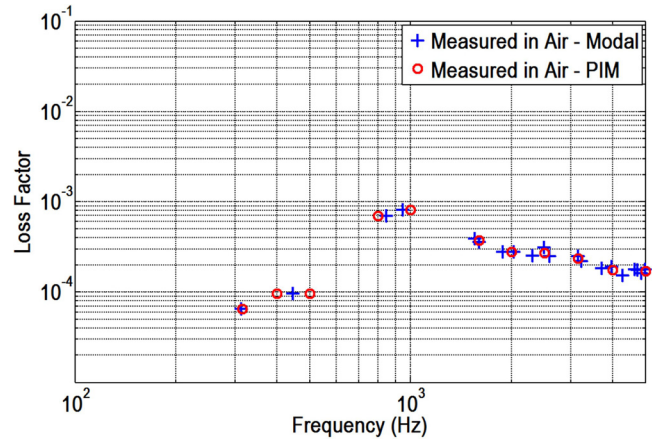


FIG. 6. (Color online) Measured modal damping for the NAB plate in air (+) with the OTO damping estimated using the power injection method (○).

losses are strongly influenced by the modal radiation losses. Since the mode near coincidence is odd-ordered and therefore has poor radiation efficiency, the radiation damping peaks at a frequency higher than the coincidence frequency. The one-third-octave (OTO) damping estimated using the power injection method is nearly identical to that of the modal damping.

Figure 7 shows the measured damping, averaged into OTO bands, once the plate is submerged in water. The

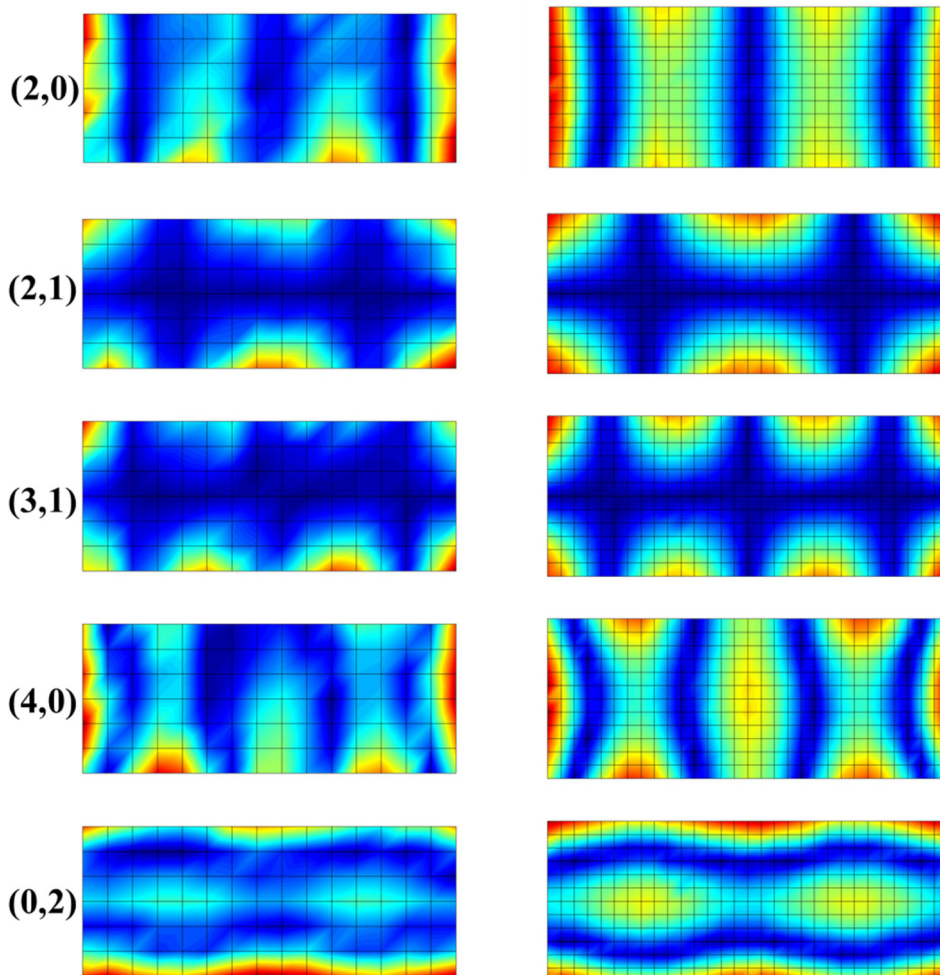


FIG. 5. (Color online) Mode shapes of the NAB plate measured in water (left) and measured in air (right).

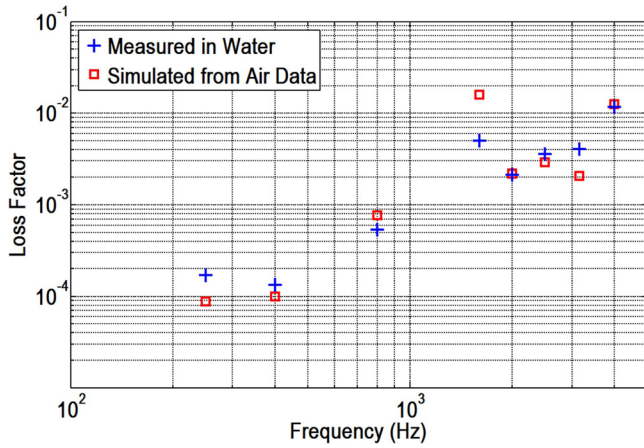


FIG. 7. (Color online) Measured modal damping (+) and estimated damping (\square) for the NAB plate in water, averaged within OTO bands. The 630 Hz and 1 kHz bands are not shown since no modes exist in those bands.

damping is higher than in air due to the increased resistance of the fluid on the plate. Additionally, the modal frequencies are now well below the plate critical frequency in water (estimated to be above 5 kHz) and damping generally increases with increasing frequency. Since the radiation damping was not removed from the in-air measurements, the simulated losses are slightly too high in the 1.6 kHz band. Additionally, the predicted damping in the 250 Hz and 3 kHz OTO band is slightly low.

Measured and simulated surface-averaged velocity is shown in Figs. 8 and 9. The effect of the fluid loading is clearly shown for the air and water measurements, and the hybrid approach compares well to the measured case. As previously discussed, the simulated damping is slightly off in two of the OTO bands. This is apparent in the velocity plots since the simulated amplitude is higher near 250 Hz and 3 kHz and lower near 1.5 kHz.

Using the computed resistance matrices, the narrow-band sound power can also be computed, as shown in Fig. 10. Since narrowband sound power estimates are difficult to make in reverberant in-water environments without special geometries (see Ref. 21), this makes the

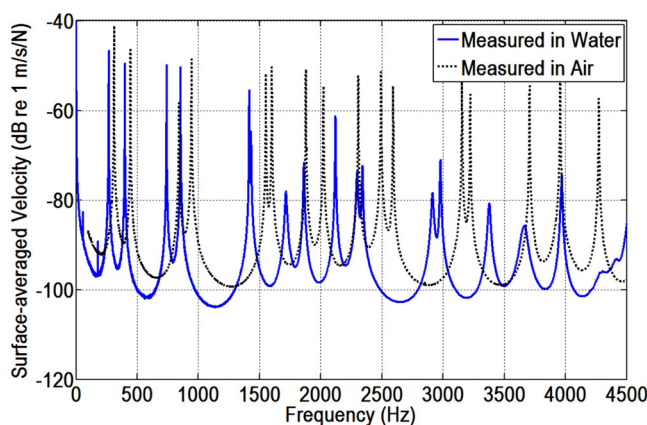


FIG. 8. (Color online) Surface-averaged velocity measured in air and in water.

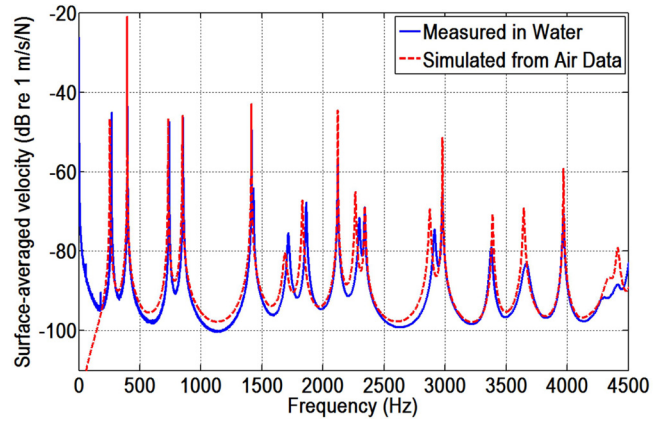


FIG. 9. (Color online) Surface-averaged velocity measured in water and hybrid approach (simulated from air data).

hybrid method more appealing as it can be applied to most geometries.

VII. LIMITATIONS

Several limitations of the hybrid method described in this paper should be listed. First, it cannot track strong frequency-dependent damping. Material damping is assumed to be fairly constant over the range where the frequencies may be shifted. Using the hybrid method on visco-elastic or porous materials may therefore over- or underestimate the damping at the fluid-loaded frequencies. Similarly, the hybrid method may not be appropriate for coupled structures, particularly if there is a strong difference in damping between the two structures. An approach similarly developed by Collery and Guyader may be more appropriate for such cases.²²

Another limitation is the need for sufficient spatial resolution for the modal analysis. If low spatial resolution is used, the mode shapes will be insufficiently resolved such that the modal resistance matrix will contain errors. There also may not be enough points to resolve the acoustic waves. Finally, the mode shapes must be reasonably estimated using plate-like elements. This is usually true when sufficient grid spacing is used. However, this is not always feasible or practical.

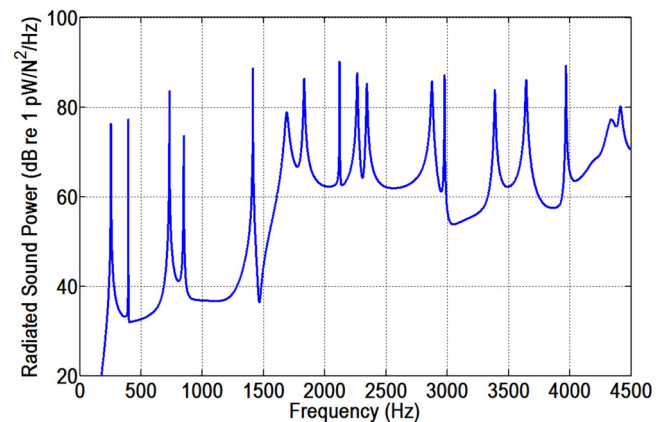


FIG. 10. (Color online) Radiated sound power for the NAB plate simulated in water using the hybrid EMA-BE approach for a unit drive on the corner.

VIII. CONCLUSION

A hybrid approach has been presented for predicting modal parameters of structures submerged in heavy fluids based on in-air measurements. The singular value decomposition is used along with RFP fitting to estimate the *in vacuo* modal parameters, including mass-normalized mode shapes. The mode shapes are then used as basis modes to compute acoustic resistance and reactance matrices using a lumped parameter BE model which accounts for external fluid loading on the structure. Elements were then created using the excitation points from modal analysis in order to determine the appropriate velocity boundary condition.

The method is evaluated using a 4.445 mm (1.75 in.) thick NAB panel by comparing natural frequencies and damping obtained using the hybrid approach to equivalent data obtained from in-water measurements. The results compare well for the majority of the modes with most natural frequencies having less than 2% error. The predicted and measured OTO loss factors are also accurate with only small errors in several bands. The in-air modes and BE-estimated mass loading and radiation damping may then be used to compute in-water structural vibration response, as well as radiated sound power for any postulated forcing function. These results reveal that the hybrid approach is a reasonably accurate method for estimating the effects of fluid-loading on structures without performing actual in-water measurements.

¹A. W. Leissa, *Vibration of Plates* (Acoustical Society of America, New York, 1993), pp. 299–300.

²R. D. Blevins, *Formulas for Natural Frequency and Mode Shape* (Krieger Publishing, Malabar, 2001).

³F. Fahy and P. Gardonio, *Sound and Structural Vibration* (Academic Press, Oxford, United Kingdom, 2007), 268 pp.

⁴E. Anderson, Z. Bai, C. Bischof, S. Blackford, J. Demmel, J. Dongarra, J. Du Croz, A. Greenbaum, S. Hammarling, A. McKenney, and D. Sorensen, *LaPack Users Guide*, 3rd ed. (Society of Industrial and Applied Mathematics, Philadelphia, PA, 1999).

⁵C. Y. Shih, Y. G. Tsuei, R. J. Allemang, and D. L. Brown, “Complex mode indication function and its applications to spatial domain parameter

estimation,” in *Proceedings of the Seventh International Modal Analysis Conference* (1989), pp. 533–540.

⁶W. H. Press, S. A. Teukolsky, W. T. Vetterling, and B. P. Flannery, *Numerical Recipes in FORTRAN* (Cambridge University Press, Cambridge, 1992), pp. 644–649.

⁷D. J. Ewins, *Modal Testing: Theory, Practice, and Applications*, 2nd ed. (Research Studies Press, Hertfordshire, England, 2001), p. 55.

⁸A. M. Iglesias, “Investigating various modal analysis techniques to estimate damping ratio,” MS thesis, Virginia Polytechnic Institute and State University, Blacksburg, VA, 2000.

⁹D. T. Wilton, “Acoustic radiation and scattering from elastic structures,” *Inter. J. Num. Meth. Eng.* **13**, 123–138 (1978).

¹⁰H. A. Schenk and G. W. Benthien, “Numerical solution of acoustic-structure interaction problems,” Naval Ocean Systems Center Technical Report No. 1263 (1989).

¹¹J. B. Fahline and G. H. Koopmann, “A lumped parameter model for the acoustic power output from a vibrating structure,” *J. Acoust. Soc. Am.* **100**(6), 3539–3547 (1996).

¹²J. B. Fahline and G. H. Koopmann, “Numerical implementation of the lumped parameter model for the acoustic power output of a vibrating structure,” *J. Acoust. Soc. Am.* **102**(1), 179–192 (1997).

¹³M. R. Shepherd and S. A. Hambric, “Minimizing the acoustic power radiated by a fluid-loaded curved panel excited by turbulent boundary layer flow,” *J. Acoust. Soc. Am.* **136**(5), 2575–2585 (2014).

¹⁴T. Terai, “On calculation of sound fields around three dimensional objects by integral equations,” *J. Sound Vib.* **69**, 71–100 (1980).

¹⁵R. Martinez, “The thin-shape breakdown (TSB) of the Helmholtz integral equation,” *J. Acoust. Soc. Am.* **90**, 2728–2738 (1991).

¹⁶J. B. Fahline, “Computing fluid-coupled resonance frequencies, mode shapes, and damping loss factors using the singular value decomposition,” *J. Acoust. Soc. Am.* **115**(4), 1474–1482 (2004).

¹⁷H. Peters, N. Kessissoglou, and S. Marburg, “Modal decomposition of exterior acoustic-structure interaction,” *J. Acoust. Soc. Am.* **133**(5), 2668–2677 (2013).

¹⁸H. Peters, N. Kessissoglou, and S. Marburg, “Modal decomposition of exterior acoustic-structure interaction problems with model order reduction,” *J. Acoust. Soc. Am.* **135**(5), 2706–2717 (2014).

¹⁹J. A. Giordano and G. H. Koopmann, “State space boundary element-finite element coupling for fluid-structure interaction analysis,” *J. Acoust. Soc. Am.* **98**(1), 363–372 (1995).

²⁰C. Q. Howard, “Modal mass of clamped beams and clamped plates,” *J. Sound Vib.* **301**, 410–414 (2007).

²¹A. R. Barnard, S. A. Hambric, and J. D. Maynard, “Underwater measurement of sound power and directivity using supersonic intensity in reverberant environments,” *J. Sound Vib.* **331**, 3931–3944 (2012).

²²O. Coltery and J. Guyader, “Solving the vibroacoustic equations of plates by minimization of error on a sample of observation points,” *J. Acoust. Soc. Am.* **127**(3), 1347–1356 (2010).